Materials Technology Reports 2024, 2(2), 1630.
https://doi.org/10.59400/mtr1630

Article

Microwave absorption properties and mechanism of novel apatite-type materials $Mn_2Gd_{7.5}Ce_{0.5}(SiO_4)_6O_2$

Haikun Liu[1,*], Xiaoming Liu[1], Ning Liu[2,3], Lefu Mei[3]

[1] National Center of Technology Innovation for Display, Guangdong Juhua Research Institute of Advanced Display, Guangzhou 510525, China
[2] School of Science, China University of Geosciences, Beijing 100083, China
[3] School of Materials Science and Technology, China University of Geosciences, Beijing 100083, China
*** Corresponding author:** Haikun Liu, liuhk@nctid.com

CITATION

Liu H, Liu X, Liu N, Mei L. Microwave absorption properties and mechanism of novel apatite-type materials $Mn_2Gd_{7.5}Ce_{0.5}(SiO_4)_6O_2$. Materials Technology Reports. 2024; 2(2): 1630. https://doi.org/10.59400/mtr1630

ARTICLE INFO

Received: 20 August 2024
Accepted: 18 October 2024
Available online: 20 November 2024

Abstract: Manganese minerals possess a high intrinsic magnetic moment, making them excellent materials for microwave absorption. Rare earth elements, with their unique electronic structures and interactions between spin electrons and orbitals, can further enhance the performance of absorbing materials. In this study, we designed a novel microwave absorbing material by incorporating manganese into an apatite structure with adjustable chemical composition. The material $Mn_2Gd_{7.5}Ce_{0.5}(SiO_4)_6O_2$, exhibiting specific microwave absorption properties, was synthesized using a high-temperature solid-phase method. The results indicate that at a sample thickness of 5 mm, the absorption frequency bandwidth below −10 dB within the 2–12 GHz range reaches 1.2 GHz, with a peak absorption of −21.78 dB. Additionally, smaller particles were prepared using the sol-gel method, achieving a peak absorption of −39.75 dB. The primary absorption mechanism for both particle types is attributed to magnetic loss. This work presents a new approach to designing microwave absorbing materials and significantly contributes to expanding the range of apatite-type materials.

Keywords: apatite structure; $Mn_2Gd_{7.5}Ce_{0.5}(SiO_4)_6O_2$; microwave absorption performance

1. Introduction

For a long time, due to the significant research value and importance of absorbing materials, researchers have made substantial progress through extensive exploration. In recent years, manganese-containing minerals, recognized for their excellent absorption properties, have drawn increasing attention from researchers [1,2]. Manganese (Mn) naturally occurs in three valence states—Mn^{2+}, Mn^{3+}, and Mn^{4+}—which can undergo redox reactions, allowing them to transform into one another [3]. Under natural conditions, the transformation between these valence states is slow and inefficient. However, under microwave irradiation, the conversion rate is significantly enhanced, which is a key reason manganese-containing minerals are applied in the field of microwave absorption [4,5]. Despite the advancements in traditional manganese-based absorbing materials, research has predominantly focused on ferrite with spinel structures, magnetoplumbite types, garnet, and perovskite structures [6]. These manganese-based absorbing materials typically exhibit relatively simple structures. To expand the research system and scope of microwave absorbing materials, the development of novel manganese-containing structures has become highly significant.

Simultaneously, researchers exploring new absorbing materials have turned their focus to the “treasure house of new materials”—Rare earth elements. Due to their unique electronic structure, interactions between electron spin and orbit, strong crystal

fields, magneto-optical effects, atomic magnetic moments, anisotropy, high magnetostrictive coefficients, and low-temperature magnetic ordering transitions, rare earth absorbing materials have broadened absorption peaks and bands, often surpassing existing theoretical limitations [7,8]. These materials have garnered significant attention for their promising applications. By combining manganese (particularly divalent manganese) with rare earth elements in the microwave absorption field, it is possible to create materials with excellent microwave absorption properties within certain crystal structures. For example, rare-earth manganese-based oxide (LSMO), a material formed from LaMnO doped with oxides such as SrO, possesses a cadmium ore structure and exhibits a giant magnetoresistance effect, making it highly suitable for the development of absorbing materials [9]. Similarly, $LaBaMnO_3$, with its perovskite-type structure, demonstrates microwave absorption properties across the 2–18 GHz range, serving as a multifunctional material for both microwave and infrared applications [10]. These materials also offer the potential for compatible camouflage in radar and infrared wave bands.

With this in mind, we focused on the apatite-structured compounds. One key advantage of the apatite structure is its highly flexible framework, which allows for a wide range of elemental substitutions, thereby offering greater control over the material's dielectric and magnetic properties. This tunability can lead to enhanced impedance matching and optimized absorption performance over a broader frequency range. For the typical apatite-structured $A_{10}[MO_4]_6O_2$, the A-site is typically occupied by divalent cations such as Ca^{2+}, Mg^{2+}, and Mn^{2+}, but rare earth ions like Eu^{2+} or alkali metal ions can also occupy this position due to isomorphic replacement [11]. Similarly, $[PO_4]^{3-}$ ions can be substituted by $[SiO_4]^{4-}$ or $[GeO_4]^{4-}$ anions under varying conditions. We therefore selected the compound $Mg_2Y_8(SiO_4)_6O_2$ with an apatite structure for substitution, using ions with appropriate radii and charges, specifically Mn^{2+}/Gd^{3+} and Mg^{2+}/Y^{3+}. After substitution, the compound $Mn_2Gd_8(SiO_4)_6O_2$ was obtained. The Mn^{2+} ions possess five unpaired electrons in their outermost layer, giving them five spin magnetic moments. This characteristic suggests that divalent manganese ions have strong theoretical microwave absorption performance. (Trivalent and tetravalent manganese ions also exhibit some microwave absorption properties.). The Mn^{2+}/Gd^{3+} cations occupy two distinct positions: one is a triple trigonal prism formed by nine oxygen atoms, and the other is an irregular pentagonal biconical polyhedron coordinated by seven oxygen atoms [12,13]. Leveraging this feature, we further incorporated Ce^{3+} ions, known for their excellent microwave absorption properties, into various cation sites to induce lattice distortion and enhance microwave absorption performance.

In this study, we report on two synthetic methods used to evaluate the microwave absorption performance of the novel apatite compound $Mn_2Gd_{7.5}Ce_{0.5}(SiO_4)_6O_2$. The crystal structure of $Mn_2Gd_{7.5}Ce_{0.5}(SiO_4)_6O_2$, synthesized using the high-temperature solid-phase method, is presented for the first time, along with its microwave absorption properties. Building on this, the compound was further synthesized using the sol-gel method, resulting in smaller particle sizes and enhanced microwave absorption performance. These findings demonstrate that this design of microwave absorbing material is both feasible and effective.

2. Experimental section

2.1. Synthesis of $Mn_2Gd_{7.5}Ce_{0.5}(SiO_4)_6O_2$

First, $Mn_2Gd_{7.5}Ce_{0.5}(SiO_4)_6O_2$ was synthesized using the conventional high-temperature solid-state method. All raw materials were of analytical grade and obtained from Xilong Chemical Co., Ltd. Manganese carbonate ($MnCO_3$, 4 mmol), gadolinium oxide (Gd_2O_3, 1.5 mmol), silicon dioxide (SiO_2, 1 mmol), and cerium oxide (CeO_2, 0.5 mmol g) were weighed according to their stoichiometric ratios. After thorough grinding in an agate mortar for 5 minutes, the ground mixture was placed in a crucible, buried in carbon, and then calcined in a muffle furnace at 1100 °C for 4 hours. Once sintering was completed and the sample was fully cooled, it was ground again in a mortar to obtain the final sample.

Second, the smaller-sized particles were prepared using the sol-gel method, with metal nitrates as raw materials and tetraethyl orthosilicate as the silicon source. The following amounts were weighed according to the stoichiometric ratio: manganese nitrate tetrahydrate (0.2 mmol), gadolinium nitrate hexahydrate (0.75 mmol), cerium nitrate hexahydrate (0.05 mmol), tetraethyl orthosilicate (0.6 mmol), and citric acid $C_6H_8O_7 \cdot H_2O$ (3.2 mmol). The mixture was stirred at 80 °C to form a wet gel, which was then dried at 120 °C for 12 hours to form a dry gel. The dry gel was then sintered at 800 °C for 10 hours to obtain a precursor, which was further sintered at 1200 °C for 5 hours to produce the final $Mn_2Gd_{7.5}Ce_{0.5}(SiO_4)_6O_2$ sample.

2.2. Materials characterization

Powder X-ray diffraction (XRD, D8 Advance diffractometer, Bruker Corporation, Germany; 40 kV and 40 mA; Cu Kα, λ = 0.15406 nm) was used for phase identification. The structural analysis employed step scanning (2 θ ranging from 3° to 130°) at a rate of 2.5 s per step, with a step size of 0.02°. To verify whether the valence state of manganese matched the design, X-ray Photoelectron Spectroscopy (XPS, Thermo Scientific) was conducted using monochromatic Al Kα irradiation (150 W). The binding energy (BE) scale was calibrated using the adventitious carbon (C 1s) core level, assigned at 284.6 eV. The morphologies of these samples were examined by a Hitachi SU4800 field-emission gun scanning electron microscope (SEM).

2.3. Microwave absorption performance measurements

The microwave absorption properties of $Mn_2Gd_{7.5}Ce_{0.5}(SiO_4)_6O_2$ were analyzed using a microwave network analyzer (N5244A, Agilent) in the 2 to 18 GHz frequency range, with the coaxial wire method in free space. The sample powder (25 wt%) was thoroughly mixed with molten wax (75 wt%), and the mixture was pressed into toroidal samples. The outer diameter of the samples was 7.00 mm, the inner diameter was 3.04 mm, and the thickness was 3 mm.

3. Result and discussions

3.1. Characterizations of materials

The material $Mn_2Gd_{7.5}Ce_{0.5}(SiO_4)_6O_2$ was successfully synthesized using both the high-temperature solid-phase method and the sol-gel method. To study the structure of the samples, the powder X-ray diffraction (XRD) was employed. In **Figure 1b**, the XRD pattern of the $Mn_2Gd_{7.5}Ce_{0.5}(SiO_4)_6O_2$ sample prepared via the high-temperature solid-phase method is presented. The crystal face indices corresponding to the diffraction peak positions at 21.765°, 22.842°, 25.879°, 28.126°, 28.966°, 31.773°, 32.172°, and 32.902° are (200), (111), (002), (102), (210), (211), (112), and (300), respectively. No new diffraction peaks were observed compared to the $Ca_2Gd_8(SiO_4)_6O_2$ standard card (JCPDS no. 28–0212), indicating that the sample retained the apatite structure, and no new phases appeared [14]. However, the diffraction peaks of the sample showed a shift to the right compared to the standard card. This shift is due to the smaller ionic radius of divalent manganese ions compared to calcium ions. When calcium ions are substituted by manganese ions, some lattice parameters decrease. Since d is inversely proportional to sin θ, and in the 2 θ range of 10° to 70°, sin θ increases monotonically, the higher the position of the characteristic peak, the smaller the d value [15]. Additionally, for the $Mn_2Gd_{7.5}Ce_{0.5}(SiO_4)_6O_2$ sample, the slight difference in atomic volume between the Ce atom and the Gd atom means that the prepared $Mn_2Gd_{7.5}Ce_{0.5}(SiO_4)_6O_2$ maintains the apatite structure. Similarly, the XRD analysis of the sample prepared by the sol-gel method (**Figure 1a**) showed the same matching diffraction peaks when compared with the standard card (JCPDS No. 28–0212), confirming that the sample also exhibits an apatite structure.

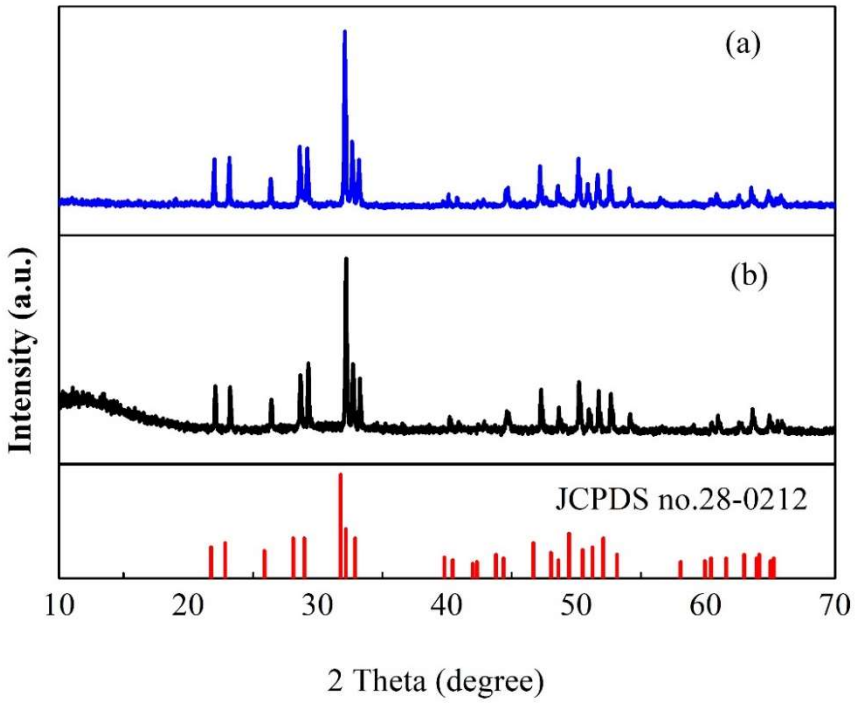

Figure 1. XRD patterns of. Mn2Gd7.5Ce0.5(SiO4)6O2 samples. **(a)** sol-gel synthesis of samples; **(b)** high temperature solid phase synthesis of samples.

The valence of manganese has a great influence on the microwave absorption properties of manganese-containing minerals due to the different number of electrons outside the nucleus, and the interactions between the different valence states also have

a certain influence on the microwave absorption properties of the materials [16,17]. In addition, due to the fact that rare earth element Ce is also a kind of variable element, the valence state of these two elements in the compound is necessarily a factor to be considered. The photoelectron survey spectrum of the $Mn_2Gd_{7.5}Ce_{0.5}(SiO_4)_6O_2$ sample is shown in **Figure 2**. The corresponding Mn element images are depicted in **Figure 2a,b**. Notably, two distinct broad peaks are observed in the $Mn_2Gd_{7.5}Ce_{0.5}(SiO_4)_6O_2$ sample, regardless of whether the sample was synthesized by the high-temperature solid-phase method or the sol-gel method. The wide survey scan of the XPS spectra revealed two peaks in the Mn 2p region at binding energies (BE) of 642.5 eV and 653.4 eV, corresponding to Mn $2p_{3/2}$ and Mn $2p_{1/2}$, respectively [18]. The BE difference (spin-orbit splitting) between the Mn $2p_{3/2}$ and Mn $2p_{1/2}$ peaks is 10.9 eV. Additionally, the fitted variance results, close to 1, suggest that Mn predominantly exists in the +2 oxidation state in the prepared samples. Meanwhile, the valence state of the cerium element on the sample surface corresponds to spin-orbit doublets characteristic of the +3 oxidation state (**Figure 2c,d**) [19].

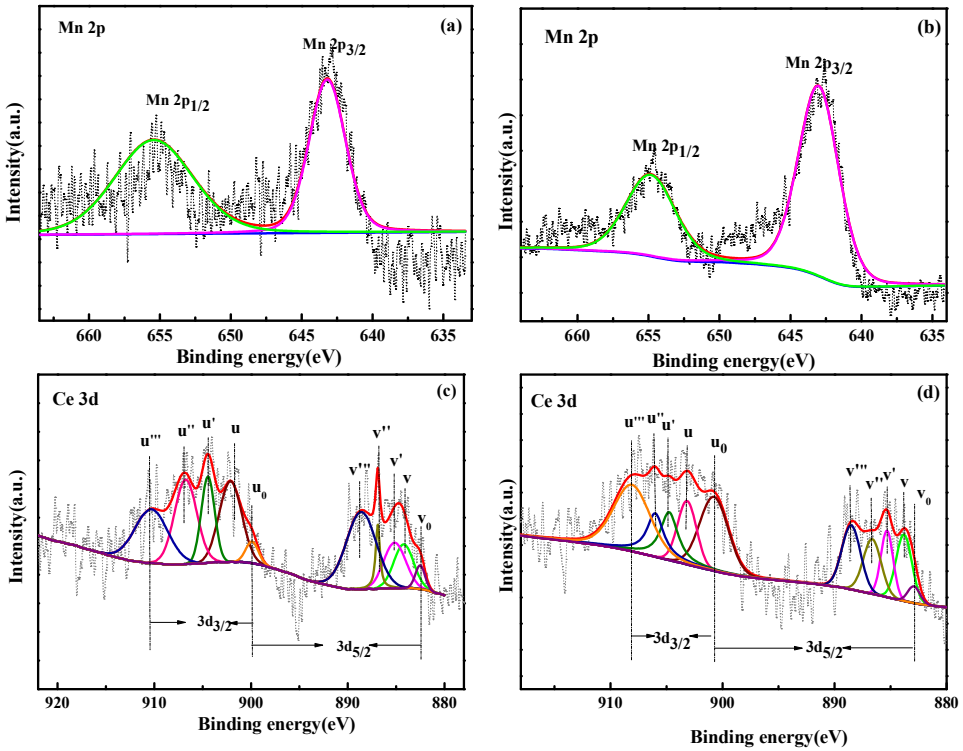

Figure 2. XPS spectra of $Mn_2Gd_{7.5}Ce_{0.5}(SiO_4)_6O_2$ samples. **(a)**, **(b)** Mn 2p of samples synthesized by high temperature solid phase method and sol-gel method; **(c)**, **(d)** Ce 3d of samples synthesized by high temperature solid phase method and sol-gel method.

The SEM images in **Figure 3a,b** show the microstructure of the samples synthesized by the high-temperature solid-state method and the sol-gel method, respectively. The particles of the sample prepared by the high-temperature solid-state method are larger and exhibit more significant agglomeration. In contrast, the sample synthesized by the sol-gel method shows a noticeable reduction in particle size, with less agglomeration. Larger particles tend to agglomerate, which prevents microwaves

from penetrating the material uniformly, thereby reducing the absorption performance. Smaller particles exhibit better dispersion, reducing agglomeration and increasing multiple scattering of microwaves within the material. This extends the propagation path of electromagnetic waves and increases the dissipation of electromagnetic energy, thereby improving microwave absorption efficiency [20].

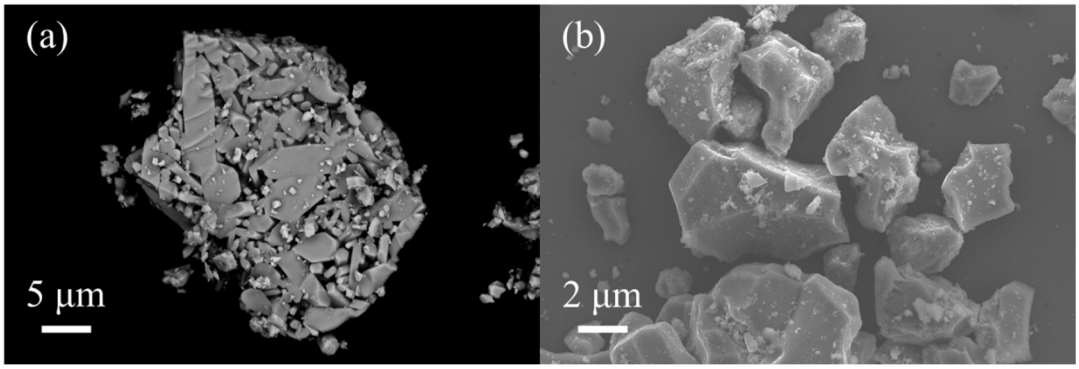

Figure 3. SEM images of the catalyst $Mn_2Gd_{7.5}Ce0.5(SiO_4)_6O_2$ samples, **(a)** high temperature solid phase synthesis; **(b)** sol-gel synthesis.

3.2. Microwave absorption performance measurements

To reveal the microwave absorption properties of the as synthesized samples, the reflection loss (RL) values of $Mn_2Gd_{7.5}Ce_{0.5}(SiO4)_6O_2$ samples were calculated using the relative complex permeability and permittivity at a given frequency and thickness layer according to the transmit line theory, which is summarized as the following equations [21]:

$$RL\ (dB) = 20 \log | (Z_{in} - Z_0)/(Z_{in} + Z_0) | \quad (1)$$

where Z_{in} and Z_0 represent the input impedance of the absorber and the impedance of free space. The absorber impedance can be calculated from the following equation [22]:

$$Z_{in} = Z_0(\mu_r/\varepsilon_r)^{1/2}\tan h\ [j\ (2\pi fd/c)\ (\mu_r\varepsilon_r)^{1/2}] \quad (2)$$

where ε_r and μ_r represent the relative complex permittivity and the relative complex permeability, respectively; f stands for the frequency; d is the thickness of toroidal shaped sample and c is the velocity of electromagnetic waves in free space. The relative complex permeability and permittivity were tested on a network analyzer with the frequency of a 2–12 GHz range.

The thickness of the sample is one of the crucial parameters that affects the intensity and position of the frequency at the RL minimum. To eliminate the influence of sample thickness, we prepared two sets of samples with thicknesses of 2, 3, 4, 5, and 6 mm. **Figure 4** illustrates the relationship between microwave reflectivity and frequency for the sample $Mn_2Gd_{7.5}Ce_{0.5}(SiO_4)_6O_2$, synthesized using the high-temperature solid-phase method and measured with vector network analysis under varying thicknesses. The data in **Figure 4a** reveals that when the sample thickness is 5 mm, the maximum absorption peak is −21.78 dB at a frequency of 5.2 GHz, with an effective microwave absorption bandwidth of 0.62 GHz. This figure clearly indicates that the intensity of microwave absorption is closely related to the thickness of the

sample. According to microwave absorption theory, sample thickness is generally proportional to microwave absorption ability; thus, within a certain range, greater thickness results in enhanced microwave absorption performance [23]. It is important to note that this relationship holds only within a specific range of sample thickness. For a wave-absorbing material, when the matching frequency exceeds the cutoff frequency, a matching thickness is established [24]:

$$t_m = c/(2\pi s_0) \quad (3)$$

where $s_0 = \mu * f_c$ (c is the light velocity, f_c is the relaxation frequency, μ_i is the initial permeability) matching thickness is only related to the performance parameter s_o of the material. When the thickness is lower than or higher than the matching thickness, the absorption coefficient of the material decreases.

The grain size of the sample is another crucial parameter that affects the microwave absorption properties of materials. Therefore, we prepared smaller samples using the sol-gel method to enhance these properties. For the samples synthesized via the sol-gel method, the same calculation method was employed. The results in **Figure 4b** indicate that the frequency position at the RL minimum shifts from higher to lower as the thickness increases, which is associated with quarter-wavelength attenuation. When the sample thickness is 6 mm, the maximum absorption peak rises to 39.75 dB at a frequency of 5.2 GHz, with an effective microwave absorption bandwidth of 0.62 GHz. This is due to the smaller grain size of the samples prepared by the sol-gel method compared to those obtained using the solid-phase method. This difference results in altered impedance matching conditions for the sample, leading to maximum microwave reflection loss at 6 mm. Additionally, the smaller size of the samples results in a larger specific surface area, more surface atoms, and more dangling bonds, which contribute to stronger interfacial polarization and increased multiple scattering.

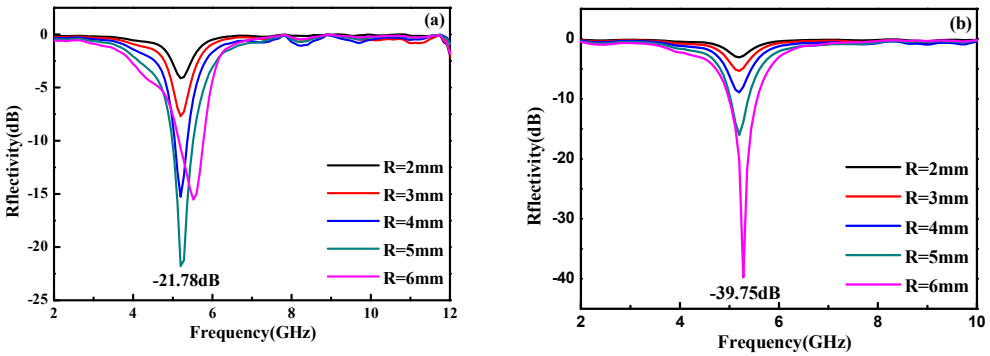

Figure 4. Frequency and microwave reflection losses for different thicknesses of $Mn_2Gd_{7.5}Ce_{0.5}(SiO_4)_6O_2$ compounds: **(a)** high temperature solid phase synthesis of samples; **(b)** sol-gel synthesis of samples.

As is well known, the synergy between the complex relative dielectric constant and permeability of a sample affects the minimum reflection loss (RL) mechanism of the material. When the dielectric constant is dominant, the reflection loss mechanism is primarily governed by dielectric loss, and the opposite is true when permeability dominates. The imaginary components of permittivity (ε″) and permeability (μ″)

indicate the material's energy dissipation capability, while the real components represent its ability to store electric (ε′) and magnetic (μ′) energy. **Figure 5** presents the complex dielectric constant, complex permeability, and tangential loss of our synthesized compounds combined with paraffin (in a 3:1 mass ratio) over a frequency range of 2 to 12 GHz. The samples were synthesized by the solid-phase method, as shown in **Figure 5a**. The real and imaginary parts of the composite dielectric constant $Mn_2Gd_{7.5}Ce_{0.5}(SiO_4)_6O_2$ increase slightly with frequency, showing no significant change in the overall composite dielectric constant. This indicates that the material exhibits no or only weak dielectric loss under the influence of a microwave alternating electric field. **Figure 5b** shows the relationship between magnetic permeability and frequency for the $Mn_2Gd_{7.5}Ce_{0.5}(SiO_4)_6O_2$. It can be observed that as the frequency increases, the real part of the magnetic permeability decreases significantly within the 4.8 GHz to 5.5 GHz range. The imaginary part of the magnetic permeability in **Figure 5b** also exhibits a sharp peak between 4.8 GHz and 5.5 GHz. This behavior, considering the trends of both μ′ and μ″, corresponds to domain resonance within this frequency range, while the remainder of the range corresponds to the relaxation spectrum. This frequency range aligns with the microwave absorption bandwidth and the frequency corresponding to the material's maximum microwave absorption peak. The observed magnetic tangent loss reaches up to 2.12 at 5.36 GHz (**Figure 5c**) and remains higher than the dielectric tangent loss across the entire frequency range, indicating that magnetic loss is the major contributor to electromagnetic loss.

The complex relative permittivity and permeability of the sample synthesized by the sol-gel method are shown in **Figure 5d–f**. The real part of the composite dielectric constant of $Mn_2Gd_{7.5}Ce_{0.5}(SiO_4)_6O_2$ slightly decreases with increasing frequency, while the imaginary part remains unchanged, indicating that the material will experience weak dielectric loss under the influence of a microwave alternating electric field. This suggests that dielectric loss is not a key factor in the microwave absorption properties of the material [25]. **Figure 5e** shows the relationship between magnetic permeability and frequency for the $Mn_2Gd_{7.5}Ce_{0.5}(SiO_4)_6O_2$. The figure shows that as frequency increases, the real part of the magnetic permeability first decreases and then increases, while the imaginary part exhibits the opposite trend. This observation is similar to the conclusion drawn from **Figure 5b**. However, the real and imaginary parts of the complex permeability (μ′, μ″) of the sample synthesized by the sol-gel method exhibit more fluctuations compared to those synthesized by the solid-phase method. This is because a decrease in particle size changes the resonance frequency of the particles, increasing both the absorption frequency and intensity. The tangent loss of $Mn_2Gd_{7.5}Ce_{0.5}(SiO_4)_6O_2$ composites in **Figure 5f** supports the same result as in **Figure 5c**, with magnetic loss still making the major contribution to electromagnetic loss.

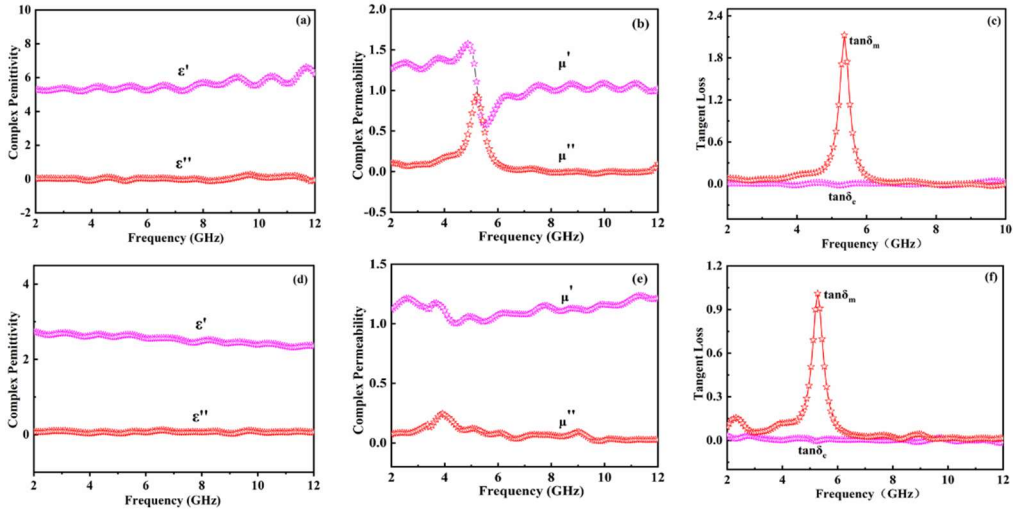

Figure 5. (a) Complex permittivity; **(b)** complex permeability; **(c)** tangent loss of high temperature solid phase synthesis of composites; **(d)** complex permittivity; **(e)** complex permeability; **(f)** tangent loss of Sol-gel synthesis of composites.

4. Conclusion

Microwave-absorbing materials with an apatite structure were successfully synthesized using both high-temperature solid-phase and sol-gel methods. The prepared samples exhibited notable microwave absorption properties, with particle sizes obtained from different preparation methods playing a crucial role in determining the microwave absorption bandwidth and depth. The microwave absorption properties of the material are primarily attributed to magnetic losses. This study provides a new perspective on the application of structural adjustment and the microwave absorption characteristics of apatite materials. The structural design of microwave-absorbing materials with rich properties and the research on apatite-structured materials in the field of microwave absorption hold significant research value and promising prospects.

Author contributions: Conceptualization, HL and LM; methodology, HL and NL; software, NL; validation, HL, XL and LM; formal analysis, NL; investigation, HL; resources, HL; data curation, NL; writing—original draft preparation, HL; writing—review and editing, NL; visualization, XL; supervision, HL; project administration, LM; funding acquisition, HL and LM. All authors have read and agreed to the published version of the manuscript.

Conflict of interest: The authors declare no conflict of interest.

References

1. Lan D, Li H, Wang M, et al. Recent advances in construction strategies and multifunctional properties of flexible electromagnetic wave absorbing materials. Materials Research Bulletin. 2023; 112630.
2. Wang D, Jin J, Guo Y, et al. Lightweight waterproof magnetic carbon foam for multifunctional electromagnetic wave absorbing material. Carbon. 2023; 202: 464–474.
3. Hu J, Liu S, Wang Y, et al. Manganese phosphate coated flaky FeSiAl powders with enhanced microwave absorbing properties and improved corrosion resistance. Materials Chemistry and Physics. 2023; 296: 127274.

4. Yang Z, Yu Z, Xu Z, et al. Molten salt-directed synthesis of carbon nanotube/C_3N_4/manganese carbodiimide (MnNCN): Novel microwave absorbing materials. Materials Research Bulletin. 2024; 175: 112757.
5. Jin L, Chen J, Zhang L, et al. Coupling dielectric and magnetic components on a ternary composite for enhancing impedance matching and microwave absorption. Ceramics International. 2024.
6. Vinnik DA, Gudkova SA, Zhivulin VE, et al. Ferrite-based solid solutions: structure types, preparation, properties, and potential applications. Inorganic Materials. 2021; 57: 1109–1118.
7. Deng Y, Wang L, Liu W, et al. Research Progress on Controllable Absorption Properties of Rare Earth Element Doped Electromagnetic Wave Absorbing Materials. Chinese Journal of Chemistry. 2024.
8. Chen Z, Li Z, Chen J, et al. Recent advances in selective separation technologies of rare earth elements: A review. Journal of Environmental Chemical Engineering. 2022; 10(1): 107104.
9. Guo J, Jing Y, Shen T, et al. Effect of doped strontium on catalytic properties of $La_{1-x}Sr_xMnO_3$ for rhodamine B degradation. Journal of Rare Earths. 2021; 39(11): 1362–1369.
10. Munazat DR, Kurniawan B, Kurita N, et al. Investigation of the impact of A-site cation disorder on the structure, magnetic properties, and magnetic entropy change of trisubstituted divalent ions in $La_{0.7}(Ba, Ca, Sr)_{0.3}MnO_3$ manganite. Physical Chemistry Chemical Physics. 2024; 26(26): 18343–18367.
11. Liu H, Liao L, Pan X, et al. Recent research progress of luminescent materials with apatite structure: a review. Open Ceramics. 2022; 10: 100251.
12. Jing XD, Li ZG, Chen ZT, et al. Effect of praseodymium valence change on the structure, magnetic, and microwave absorbing properties of M-type strontium ferrite: the mechanism of influence of citric acid dosage and calcination temperature. Materials Today Chemistry. 2023; 30: 101537.
13. Khanvilkar MB, Nikumbh AK, Pawar RA, et al. Effect of divalent/trivalent doping on structural, electrical and magnetic properties of spinel ferrite nanoparticles. Engineered Science. 2023; 22: 850.
14. Fu J, Liu N, Mei L, et al. Synthesis of Ce-doped $Mn_3Gd_{7-x}Ce_x(SiO_4)_6O_{1.5}$ for the enhanced catalytic ozonation of tetracycline. Scientific Reports. 2019; 9(1): 18734.
15. Gupta I, Singh D, Singh S, et al. Study of structural and spectroscopic characteristics of novel color tunable yellowish-white Dy^{3+} doped $Gd_4Al_2O_9$ nanophosphors for NUV-based WLEDs. Journal of Molecular Structure. 2023; 1272: 134199.
16. Tian F, Gao Y, Wang A, et al. Effect of Mn substitution on structural, magnetic and microwave absorption properties of Co_2Y hexagonal ferrite. Journal of Magnetism and Magnetic Materials. 2023; 587: 171229.
17. Yue J, Cheng L, Xiong J, et al. Effect of neodymium doping on structure, magnetic properties and microwave absorption performance of $SrMnO_3$. Journal of Rare Earths. 2024; 42(2): 354–363.
18. Yin Y, Yan S, Ni Z, et al. Economical synthesized Mn_3O_4/biomass-derived carbon from vegetable sponge composites and its excellent supercapacitive behavior. Biomass Conversion and Biorefinery. 2023; 13(13): 12115–12124.
19. Dhandapani P, Nayak PK, Maruthapillai A. Improved electrochemical performance and charge storage mechanism of $NiMnCoO_4$ by XPS study. Materials Chemistry and Physics. 2023; 297: 127287.
20. Zheng Q, Yu M, Wang W, et al. Enhanced microwave absorption performance of Fe/C nanofibers by adjusting the magnetic particle size using different electrospinning solvents. Ceramics International. 2020; 46(18): 28603–28612.
21. Quan B, Gu W, Sheng J, et al. From intrinsic dielectric loss to geometry patterns: Dual-principles strategy for ultrabroad band microwave absorption. Nano Research. 2021; 14: 1495–1501.
22. Lei C, Du Y. Tunable dielectric loss to enhance microwave absorption properties of flakey FeSiAl/ferrite composites. Journal of Alloys and Compounds. 2020; 822: 153674.
23. Elmahaishi MF, Ismail I, Muhammad FD. A review on electromagnetic microwave absorption properties: their materials and performance. Journal of Materials Research and Technology. 2022; 20: 2188–2220.
24. Yang SJ, Park KT, Im J, et al. Ultrafast 27 GHz cutoff frequency in vertical WSe_2 Schottky diodes with extremely low contact resistance. Nature communications. 2020; 11(1): 1574.
25. Wang F, Liu Y, Zhao H, et al. Controllable seeding of nitrogen-doped carbon nanotubes on three-dimensional Co/C foam for enhanced dielectric loss and microwave absorption characteristics. Chemical Engineering Journal. 2022; 450: 138160.